ELSEVIER

Chemical Engineering Journal 81 (2001) 231–250

Chemical Engineering Journal

www.elsevier.com/locate/cej

Parametric study on the production of phosphoric acid by the dihydrate process

Samir I. Abu-Eishah*, Nizar M. Abu-Jabal

Department of Chemical Engineering, Jordan University of Science and Technology, Irbid 22100, Jordan

Received 22 March 1999; received in revised form 15 March 2000; accepted 5 April 2000

Abstract

In this work a computer program has been developed to simulate a three-CSTR pilot plant leaching process of phosphate rock with sulfuric acid for the production of phosphoric acid and precipitation of calcium sulfate dihydrate as a byproduct. The simulation model has been examined with real experimental data obtained from the Jordan Phosphate Mines Company (JPMC), a phosphoric acid pilot plant at Rusaifa, Jordan. The predicted results are in very good agreement with the experimental data with a relative absolute error of less than 3.5%.

A parametric study has been made to find the optimum operating conditions of the pilot plant for a given phosphate rock feed flow rate, chemical composition, and particle size distribution. The effect of varying reactor(s) temperature, sulfuric acid feed rate, agitator–impeller speed, ratio of slurry recycle to feed rate, and ratio of return acid to feed rate have been investigated. A reactor temperature of 80°C, slurry recycle to feed ratio of 80, and return acid to feed ratio of 2.5 have been found to give best results. The optimum conditions for sulfuric acid feed rate and agitator speed are determined only from power limitations and economics of the plant itself.

Keywords: Phosphoric acid; Dihydrate process; Pilot plant; Modeling and simulation; Parametric study

1. Introduction

Practically almost all phosphoric acid needed for the fertilizer industry is produced by wet processes. In many of these processes, the raw phosphate ore is converted into phosphoric acid and calcium sulfate dihydrate (gypsum) by adding a mixed solution of sulfuric and phosphoric acids to the reactor [1].

The rapid expansion in the manufacture of phosphoric acid by the wet processes is a result of the increased demand for high-grade fertilizers, and the energy saving in the wet processes compared with thermal processes [2]. Selection of the wet process type depends on a number of factors such as the cost of the phosphate rock, cost and availability of sulfuric acid (and steam), intended use of the produced phosphoric acid, and whether or not there is a use for the byproduct gypsum [3].

The main chemical reaction involved in the wet process may be represented by the following equation using pure fluorapatite to represent the phosphate rock:

$$3Ca_3(PO_4)_2 \cdot CaF_2 + 10H_2SO_4 + 10nH_2O \rightarrow 6H_3PO_4 + 10CaSO_4 \cdot nH_2O + 2HF \quad (1)$$

where $n = 0, \frac{1}{2}$, or 2, depending on the hydrate form in which the calcium sulfate crystallizes. This reaction represents the net result of a two-stage reaction [4]

$$3Ca_3(PO_4)_2 \cdot CaF_2 + 14H_2SO_4 \rightarrow 10Ca(H_2PO_4)_2 + 2HF \quad (2)$$

$$Ca(H_2PO_4)_2 + H_2SO_4 + nH_2O \rightarrow 2H_3PO_4 + CaSO_4 \cdot nH_2O \quad (3)$$

In the first stage, phosphoric acid (from recycled slurry stream) attacks the phosphate ore particles to form soluble monocalcium phosphate. In the second stage, the formed monocalcium phosphate reacts with sulfuric acid in the solution to form phosphoric acid and insoluble calcium sulfate. These two stages usually take place simultaneously in a single reactor. However, many other side reactions are involved [5], among which is the reaction of calcium carbonate whose content in the phosphate rock determines to a great extent

* Corresponding author. Address: Department of Chemical Engineering, University of Bahrain, PO Box 32038, Isa Town, Bahrain. Tel.: +973-681234; fax: +973-684844.

1385-8947/01/$ – see front matter
PII: S1385-8947(00)00166-2

Nomenclature

B_j	mass fraction of gypsum per unit mass of slurry in reactor j (kg/kg)
C_{CS}	concentration of $CaSO_4$ (kg/m^3)
C_{CS}^*	equilibrium concentration of $CaSO_4$ (kg/m^3)
C_{PA}	concentration of H_3PO_4 (kg/m^3)
C_{SA}	concentration of H_2SO_4 (kg/m^3)
D_I	impeller diameter (m)
D_T	reactor (tank) diameter (m)
D_v	diffusion coefficient of H^+ ions in solution (m^2/h)
$E(t)$	exit age distribution function (1/h)
$f(R)$	input size distribution function (kg/kg m)
F	stream mass flow rate (kg/h)
F_A	H_2SO_4 feed mass flow rate (kg/h)
F_F	phosphate rock mass feed flow rate (kg/h)
F_G	gypsum mass flow rate (kg/h)
F_P	phosphoric acid product mass flow rate (kg/h)
F_{PA}	theoretical mass flow rate of 100% H_3PO_4 produced (kg/h)
F_R	return acid mass flow rate (kg/h)
F_{RS}	slurry recycle mass flow rate (kg/h)
F_V	makeup water mass flow rate (kg/h)
F_W	wash water mass flow rate (kg/h)
G	degree of supersaturation (dimensionless)
K	constant in the linear crystal growth rate (m^4/h kg)
K_L	physical mass transfer coefficient of H^+ in solution (m/h)
L	characteristic dimension of the crystal (m)
m	mass of slurry in reactor (kg)
$m_{HF,T}$	total mass flow rate of HF produced from all vessels (kg/h)
$m_{HF,L}$	mass flow rate of HF converted to H_2SiF_6 in the liquid phase (kg/h)
$m_{HF,V}$	mass flow rate of HF released as a gas (kg/h)
m_{CO_2}	mass flow rate of CO_2 produced (kg/h)
M_C	molecular weight of CaO (kg/kmol)
M_F	molecular weight of F (kg/kmol)
M_G	molecular weight of $CaSO_4$ (kg/kmol)
M_{G2}	molecular weight of $CaSO_4{\cdot}2H_2O$ (kg/kmol)
M_{HF}	molecular weight of HF (kg/kmol)
M_P	molecular weight of P_2O_5 (kg/kmol)
M_{PA}	molecular weight of H_3PO_4 (kg/kmol)
M_S	molecular weight of SO_4 (kg/kmol)
M_{SA}	molecular weight of H_2SO_4 (kg/kmol)
Q_j	total volumetric flow rate into Reactor j (m^3/h)
r	phosphate particle radius at any time (m)
R	uniform radius of particles entering the reactor (m)
R_{avg}	average radius of particles entering the reactor (m)
R_{max}	maximum radius of phosphate rock particles (m)
R_{min}	minimum radius of phosphate rock particles (m)
Re	Reynolds number (dimensionless)
Sc	Schmidt number (dimensionless)
t	dissolution time of a single particle (h)
t_{avg}	average or mean residence time (h)
T_R	complete dissolution time of a single particle of radius R (h)
T	temperature (°C)
V	reactor volume (m^3)
V_g	mass flow rate of a gas stream (kg/h)
V_T	total mass flow rate of gas released from all vessels (kg/h)
W_s	total mass flow rate into reactor (kg/h)
X	conversion degree in a reactor (kg/kg)
X_A	mass fraction of H_2SO_4 in sulfuric acid feed (dimensionless)
X_C	mass fraction of CaO in a reactor (dimensionless)
X_{CF}	mass fraction of CaO in phosphate feed (dimensionless)
X_{CG}	mass fraction of CaO in gypsum (dimensionless)
X_{CO_2}	mass fraction of CO_2 in phosphate feed (dimensionless)
X_{CP}	mass fraction of CaO in phosphoric acid product (dimensionless)
X_{CS}	mass fraction of $CaSO_4$ in a reactor (dimensionless)
X_{FF}	mass fraction of F in phosphate feed (dimensionless)
X_{GR}	mass fraction of gypsum in return acid (dimensionless)
X_{ORG}	mass fraction of organic matter in phosphate feed (dimensionless)
X_P	mass fraction of P_2O_5 in a reactor (dimensionless)
X_{PA}	mass fraction of H_3PO_4 in a reactor (dimensionless)
X_{PF}	mass fraction of P_2O_5 in phosphate feed (dimensionless)
X_{PG}	mass fraction of P_2O_5 in phosphogypsum (dimensionless)
X_{PR}	mass fraction of P_2O_5 in return acid (dimensionless)
X_S	mass fraction of SO_4 in H_2SO_4 feed (dimensionless)
X_{SA}	mass fraction of H_2SO_4 in a reactor (dimensionless)
X_{SF}	mass fraction of SO_4 in phosphate feed (dimensionless)

X_{SG} mass fraction of SO_4 in gypsum (dimensionless)
X_{SP} mass fraction of SO_4 in H_3PO_4 product (dimensionless)

Greek letters
α part of anhydrous sulfuric acid per part of rock for stoichiometric acidulation (kg/kg)
β constant exponent in Eq. (17) characteristic of particle size distribution
μ viscosity of reaction solution (kg m/h)
υ_L linear crystal growth rate (m/h)
υ_e crystal growth rate (kg/h m^2)
υ_M dissolution rate of phosphate rock per unit of particle surface (kg/h m^2)
ρ density of reaction mixture (kg/m^3)
ρ_{G2} density of produced gypsum crystals (kg/m^3)
ρ_M density of mineral feed (kg/m^3)
Φ_M mineral particle shape factor (dimensionless)
$\psi_j{}^0$ nuclei population density in reactor j (#/kg m)
ψ_j crystal population density in reactor j (#/kg m)
ω impeller speed (rph)

Abbreviations
eq equilibrium

Subscripts
j reactor number

the crystal size of the apatite. It also determines the pore structure and hence the reactivity of the phosphate rocks [6].

As the phosphate ore particles dissolve in the reactor, supersaturation of calcium sulfate occurs, thereby leading to gypsum crystallization that involves both nucleation and crystal growth [7]. The form in which the calcium sulfate crystallizes (i.e., type of process) depends on the reaction temperature and on the acid concentration in the reaction system itself. At a temperature range of 70–80°C and moderate acid concentrations, the calcium sulfate crystallizes in the gypsum (dihydrate: $CaSO_4{\cdot}2H_2O$) form, as it is the case in this work. At higher acid concentrations and temperatures (>80°C), the hemihydrate ($CaSO_4 \cdot \frac{1}{2}H_2O$) is formed, and at still higher acid concentrations and temperatures (90–100°C), the anhydrite ($CaSO_4$) is formed [3].

Two main types of wet processes are available: single-stage processes and recrystallization processes. The single-stage processes are those in which there is only one reaction–recrystallization step, regardless of the form in which the byproduct gypsum is formed. The most common routes of the single-stage processes are the dihydrate and the hemihydrate processes.

The main advantage of the hemihydrate process is the low grinding requirements compared with the dihydrate route, but generally the efficiency of P_2O_5 recovery in the hemihydrate process is lower. Generally, the P_2O_5 efficiency of recovery of a dihydrate process is in the range 95–98%, but for a hemihydrate process it is usually below 95%. This is mainly because, in order to maintain the higher acid concentration needed to ensure that the calcium sulfate crystallizes as hemihydrate, it is not to wash the filter cake as thoroughly as in the dihydrate process [3].

The major advantages of the single-stage dihydrate process appear to be related to its flexibility and reliability, since it is the most popular and vast literature on operating conditions exists. Also in this process, more moisture is permissible in the phosphate feed, and there is more tolerance to the use of weak sulfuric acid, since the overall water balance in the system is not so critical [3].

Recrystallization processes have the general aim of improving the overall efficiency of P_2O_5 recovery, which includes greater purity of the final filter cake, and in some cases, the production of a high-strength acid directly (i.e., without the need for further concentration). These processes include the two-stage hemihydrate–dihydrate and dihydrate–hemihydrate processes as well as the three-stage hemi/di/hemihydrate process [3]. The recrystallization step involves the addition of dilute sulfuric acid to the gypsum crystals (filter cake) for sufficient time to recrystallize them from one structure to another (i.e., from hemihydrate to dihydrate or the reverse). In this step most of the P_2O_5 trapped in the cake is released and recovered.

Acidulation of the phosphate rock by sulfuric acid to produce phosphoric acid is an old process. A broad experimental knowledge has been found in industrial plants and laboratories. However, modeling of the phosphoric acid reactor, which is the main unit in the wet process, remains a difficult task. As a result, very few papers in the literature use the modeling approach, which still requires important modifications, in order to understand the system performance [7].

Gioia et al. [8] put forward a multi-reactor mathematical model, based on material and population balances, for calcium sulfate crystallization in the hemihydrate state ($CaSO_4 \cdot \frac{1}{2}H_2O$) for which kinetics data are, somewhat, available in literature. The Gioia et al. model consists of *N*-CSTRs in series (dissolution–crystallizer reactors). In their model, the phosphate rock, the sulfuric acid and the recycle from the filter (return acid) are all fed to the first reactor. They ran their theoretical model as a single reactor at 120°C with 10% excess of H_2SO_4 and found that crystallization is the limiting step in the reaction. They mentioned that the recycle ratio (ratio of return acid flow rate to H_2SO_4 feed rate) controls the supersaturation in the reactors and the degree of supersaturation, namely, the possibility of the covering of the mineral particles by the formed $CaSO_4 \cdot \frac{1}{2}H_2O$. They also mentioned that the growth rate of the crystals and the nucleation rate are strongly influenced by this recycle ratio. Unfortunately, Gioia et al. presented no comparison between experimental and model computed results, so their model remains purely theoretical [7].

Shakourzadeh et al. [7] simulated a dihydrate process consisting of a single reactor–crystallizer system at 70°C with

a recycle from the filter. They compared their results with the output from a continuous lab-scale pilot reactor fed with iron-rich Togo apatite. Their method of solving the model approaches that of Gioia et al. [8] with nearly similar material and population balance equations and correlations. They mentioned that as the phosphate rock dissolves in the reactor, supersaturation of calcium sulfate occurs, thereby leading to gypsum crystallization, which involves both nucleation and crystal growth. They assumed that the Ca^{2+} concentration is at its equilibrium value (and that it has no significant effect on the computed results). They also assumed that the concentration of H^+ ions at the solid–liquid interface is much smaller than that in the bulk liquid and concluded that the chemical reaction at the solid–liquid interface is fast and the leaching of the phosphate rock takes only a few minutes residence time.

Three rate-determining steps in the reactions involved in the wet process have been suggested [9]: (1) diffusion of the calcium ions away from the phosphate ore particles, (2) diffusion of the hydrogen ions into these particles, and (3) chemical reaction of the acid(s) with the phosphate ore particles. Gilbert and Moreno [10] and Slack [6] proposed that the rate of reaction is a function of H^+ ions concentration, surface area of the phosphate ore particles, diffusion through the liquid film at the particles surface, and reaction temperature. Shakourzadeh et al. [7] mentioned that the rate-determining step is the diffusion of H^+ ions toward the solid particle. van der Sluis et al. [9], in their work on the digestion of phosphate in phosphoric acid, determined that the Ca^{2+} ion diffusion from the surface of the ore into the bulk of the solution is the rate-limiting step. For degrees of supersaturation above 2.5 (see Eqs. (34) and (35) for definition), it is claimed that the diffusion of reactants and products through the formed solid layer to/or from the interface of the unreacted core (i.e., the reaction surface) controls the overall dissolution process [6,10]. Jansen et al. [1] attributed the diversity of data and opinions on this subject to the unavoidable conversion of the various forms of $CaSO_4$ at prolonged equilibrium times from $CaSO_4 \cdot \frac{1}{2}H_2O$ (unstable) $\rightarrow$ $CaSO_4 \cdot 2H_2O$ (metastable) $\rightarrow$ $CaSO_4$(stable).

For the crystallization process of the byproduct gypsum, Slack [6] mentioned that in order to form a nucleus, the reacting ions and molecules must be brought to an activation energy sufficient to cross a certain energy barrier. However, under the conditions of the common phosphoric acid processes, very few ions and molecules attain energy sufficient to cross such barrier. Thus, the introduction of externally grown seed crystals is sometimes used to promote a certain crystal habit. Hignett [12] and Gilbert and Moreno [10] suggested a large volume of slurry recirculation from the last compartment of the plant to the first. The average lifetime of a single phosphate particle in a typical reaction system may range from 0.25 to 3 min [12].

Gilbert and Moreno [10] said that it is essential to grow the gypsum crystals to become satisfactory for filtration. Here, the rate of crystal growth depends in part on the rate of supply of calcium ions to the solution, which is in turn governed by the rate of dissolution of the phosphate ore particles. Amin and Larson [11] mentioned that $CaSO_4 \cdot \frac{1}{2}H_2O$ has a higher relative growth rate and a lower relative nucleation rate than does $CaSO_4 \cdot 2H_2O$. Thus, the latter (gypsum) needs longer residence time and a more precise condition control would be necessary to obtain the desired crystal form and the growth rate of these crystals, in general, increases with the increase of the reaction temperature. Shakourzadeh et al. [7] mentioned that the average crystal growth rate increases substantially as the residence time is decreased (due to increasing supersaturation) and that the shape and dimensions of the crystals depend on the SO_4^{2-} concentration in the solution.

In this work a model-based computer program will be developed to simulate a three-CSTR pilot plant leaching process of phosphate rock with sulfuric acid for the production of phosphoric acid and precipitation of calcium sulfate dihydrate as a byproduct. The simulation model will be examined with real experimental data obtained from the Jordan Phosphate Mines Company (JPMC), a phosphoric acid pilot plant at Rusaifa, Jordan. A parametric study will then be made to find the optimum operating conditions of the pilot plant for a given phosphate rock feed flow rate, chemical composition, and particle size distribution. The effect of varying reactor(s) temperature, sulfuric acid feed rate, agitator–impeller speed, ratio of slurry recycle to feed rate, and ratio of return acid to feed rate will be investigated.

2. Analysis of the dihydrate wet process

2.1. Description of the JPMC pilot plant

The mathematical model used in this work represents a 10–16 kg/h capacity pilot plant used by the JPMC to produce phosphoric acid by the dihydrate process. However, with some changes in the flow configuration and in the operating conditions, the same pilot plant can also be used to produce phosphoric acid by other wet processes [13]. As shown in the schematic diagram in Fig. 1, the pilot plant consists of three isothermal CSTRs (R_1, R_2 and R_3) and one filter–feed tank (R_4), all connected in series. The suspension mixture overflows from one reactor to another. These reactors represent the core of the plant where chemical reactions, crystallization, and other phenomena take place. The reactant fluid that is made of a suspension of solid particles in a liquid (i.e., the slurry) is kept under relatively high speed of agitation in order to keep even the largest particles suspended [9].

The phosphate rock feed (F_F) is fed to the first reactor (R_1). Sulfuric acid feed (F_A) and return acid from the filter (F_R) are mixed together in a mixing box and introduced into the third reactor (R_3). In this way, most of the water soluble P_2O_5 losses can be recovered back into the process by circulating part of the dilute filtrate (acid) back to previous

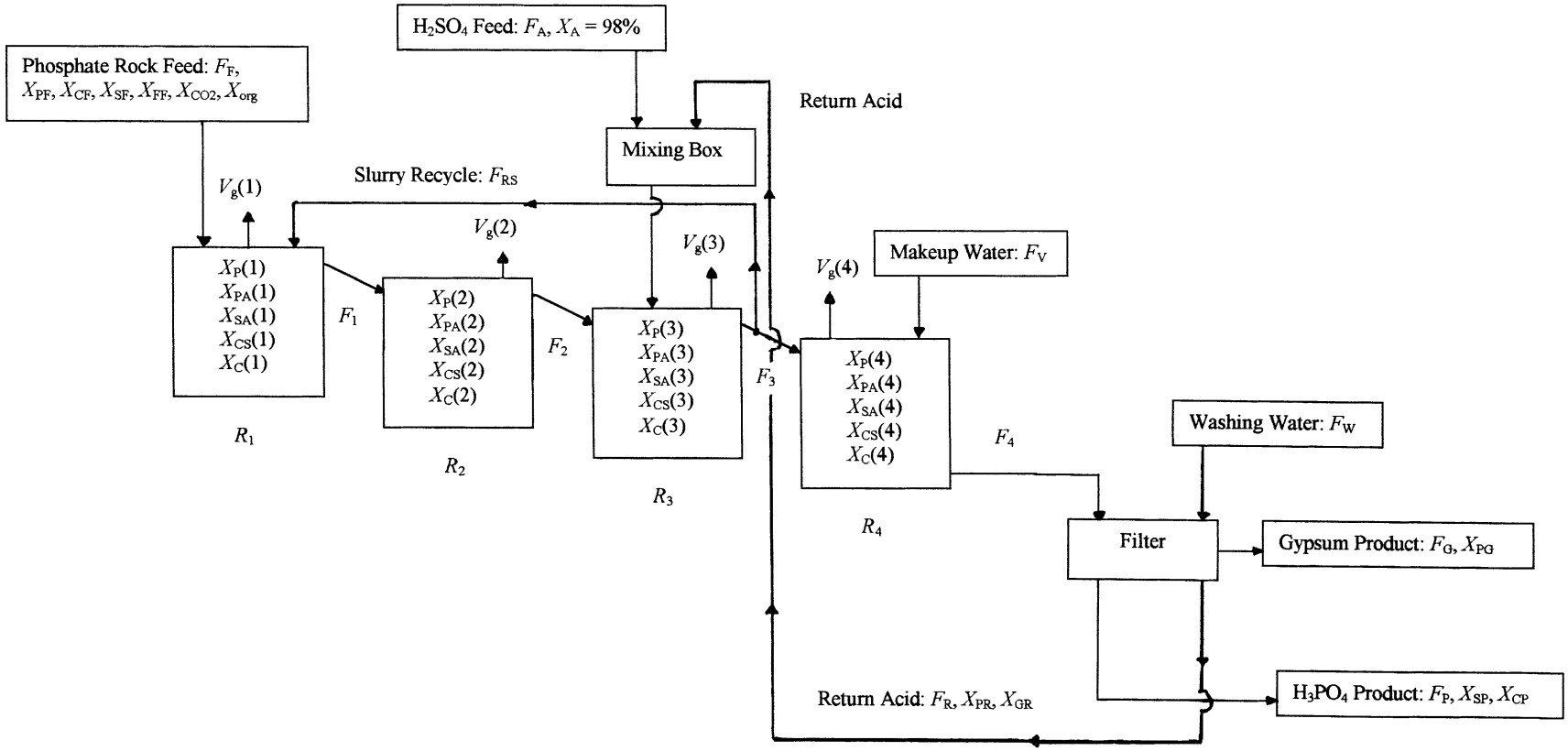

Fig. 1. Flowsheet of the JPMC pilot plant for production of phosphoric acid.

stages of filter washing and the remaining part for the dilution of concentrated sulfuric acid feed before it enters the reactor(s). As recommended, large amount of slurry (F_{RS}) is recycled from the third reactor to the first [4,10].

The fluorine gas evolved during reaction (as SiF_4 and HF) as well as CO_2 gas coming from decomposition of carbonates and oxidation of organic matter are vented to the atmosphere (in the JPMC pilot plant) or discarded to a suitable scrubbing system in industrial plants. The overall gas mass flow rate from reactor or tank j is $V_g(j)$. CO_2 gas may form some kind of foam on the reaction surface in the reactors, so a defoamer is added in small amounts to control the foam formed during processing. The output stream from the third reactor, F_3, is introduced to the filter feed tank (R_4), which provides a constant head of slurry for the filtration process.

A stream of makeup water, F_V, may be added to compensate for water losses through evaporation from the reactors (no makeup water is used here). Washing water, F_W, is added to the filter, which is the last step in the process, where gypsum stream, F_G, and product acid stream, F_P, are obtained. Some of the product acid is recycled as a return acid, F_R, to the third reactor (R_3) as mentioned before for reaction initiation [4]. No additional cooling by artificial means (air or vacuum cooling) is required here, because the excess heat released from the reactions is just sufficient to cover the natural heat loss [6].

2.2. Model formulation

The process consists of a reaction on the phosphate particles by sulfuric acid producing a solution mainly composed of calcium sulfate and phosphoric acid. The stoichiometry of the overall dissolution reaction depends on the chemical composition of the phosphate rock. The calcium sulfate separates by crystallizing as $CaSO_4{\cdot}2H_2O$ if the values of the temperature and composition (H_3PO_4 and H_2SO_4) existing in the solution are, as mentioned earlier, in a well-defined range.

The analysis followed in this work is based mostly on the general results and methods of transport phenomena, chemical kinetics, and material and population balances, similar to those of Gioia et al. [8] and Shakourzadeh et al. [7]. Because of the complexity of the process, the limited basic experimental data reported in the literature and the limitations of mathematics, the model is somewhat idealized and is expected to give reliable representation of the influence of some of the variables that affect the performance of the process.

Since the reactant fluid is made up of a suspension of solid particles in a liquid (slurry), the use of continuous stirred tank reactors (CSTR) is most appropriate. In this work, we are mainly interested in the reactor–crystallizer where dissolution and crystallization take place. The material balance equations for the various parts of the JPMC pilot plant are presented in Appendix A. Other equations and correlations for reaction kinetics, crystallization and popular balances are presented next.

Through the present analysis, a flow pattern characterized by perfect macromixing and segregation for solid particles has been postulated. Perfect macromixing implies an exit age distribution function, $E_j(t)$ given by

$$E_j(t) = \frac{1}{t_{avg}} \exp\left(\frac{-t}{t_{avg}}\right) \tag{4}$$

where t is the dissolution time of a single particle (h). t_{avg} is the mean residence time (h) defined as "mass of slurry in reactor j/mass flow rate of suspension to reactor j", and is given by

$$t_{avg} = \frac{m}{W_s} = \frac{\rho V}{W_s} \tag{5}$$

where m is the mass of slurry in reactor (kg), W_s the total mass flow rate into reactor (kg/h), V the reactor volume (m^3), and ρ the density of reaction mixture (kg/m^3).

The above ideal flow pattern is, in general, a good approximation of real mixed reactors. However, for a different flow pattern, the analysis given here may be easily modified by using a more appropriate $E_j(t)$ function than that given by Eq. (4).

2.2.1. Dissolution mechanism

Assuming that the phosphate rock particles are spherical in shape, one can visualize the following steps occurring during the dissolution of the phosphate rock [8].

1. At the solid/liquid interface, the salts that are contained in the mineral dissolve and dissociate. At this interface, thermodynamic equilibrium whose conditions are regulated by the solubility products is postulated.
2. The reactant H^+, derived from H_2SO_4 dissociation, diffuses from the core of the liquid toward the liquid/solid interface.
3. H^+ ions react with the main constituents of the rock. Neglecting other minor reactions, the main reactions taking place in the liquid phase are

$$\begin{aligned} &PO_4^{3-} + 3H^+ \rightarrow H_3PO_4 \\ &F^- + H^+ \rightarrow HF \\ &CO_3^{2-} + 2H^+ \rightarrow H_2CO_3 \rightarrow H_2O + CO_2 \end{aligned} \tag{6}$$

4. All reaction products diffuse back into the main body of the liquid.

The above reactions occur by proton transfer mechanism and therefore can be assumed to be instantaneous with respect to diffusion. The overall dissolution process is thus controlled by the diffusion of reactants toward a reaction plane. This situation is analogous to that encountered in the process of gas absorption with instantaneous chemical reaction [8]. On the basis of this analogy, since the physical solubility of the rock (in water) is much smaller than the H_2SO_4 concentration, the following expression can be written for the dissolution rate of a single particle (kg of

H_2SO_4 consumed per hour per m^2 of particle):

$$\upsilon_M = K_L C_{SA}(j) \tag{7}$$

where K_L is the physical mass transfer coefficient of H^+ ions in solution (m/h), and $C_{SA}(j)$ the H_2SO_4 concentration in the bulk of the liquid in reactor j (kg/m^3). The dissolution time of a single phosphate particle, t, in reactor j from an initial average radius R_{avg} to a final radius r is given by

$$t = \frac{-\Phi_M \rho_M \alpha}{C_{SA}(j)} \int_{R_{avg}}^{r} \frac{dr}{K_L(r)} \tag{8}$$

where Φ_M is the mineral particle shape factor (dimensionless), ρ_M the density of mineral feed (kg/m^3), α the part of anhydrous sulfuric acid per part of rock for stoichiometric acidulation (kg/kg), r the phosphate particle radius at any time (m), and R_{avg} the average radius of particles entering the reactor (m).

The shape factor Φ_M is defined here as the ratio of the surface area of a sphere of volume equal to that of the particle to the surface area of the particle. The value of α here accounts for all species in the phosphate rock that react with sulfuric acid.

Assuming a height of liquid equal to the reactor diameter, which is almost true for this study, the physical mass transfer coefficient, K_L, is given by [8]

$$\ln\left(\frac{2rK_L(r)}{D_v\, Sc^{0.33}}\right) = 0.479 \ln\left(\frac{6r}{D_T}\right) + 0.359 \ln Re - 0.533 \tag{9}$$

where D_T is the tank (reactor) diameter (m), D_v the diffusion coefficient of H^+ ions in solution (m^2/h), Re the Reynolds number ($= \rho\omega {D_I}^2/\mu$) which is also dimensionless, Sc the Schmidt number ($=\mu/\rho D_v$) which is dimensionless, D_I the impeller diameter (m), ω the impeller speed (rph), μ the viscosity of reaction solution (kg m/h), and ρ the density of reaction solution (kg/m^3).

After some mathematical manipulation, Eq. (9) becomes

$$K_L = \left(\frac{0.69219 D_v\, Sc^{0.33}\, Re^{0.359}}{{D_T}^{0.479}}\right)\left(\frac{1}{r}\right)^{0.521} \tag{10}$$

For $r = R_{avg}$, and $B = 0.69219 D_v\, Sc^{0.33}\, Re^{0.359}/{D_T}^{0.479}$, Eq. (10) becomes

$$K_L = B\left(\frac{1}{R_{avg}}\right)^{0.521} \tag{11}$$

After setting $A = -\Phi_M \rho_M \alpha / C_{SA}(j)$ and substituting for K_L from Eq. (11), the integration of Eq. (8) gives

$$t = 0.65746\frac{A}{B}(r^{1.521} - {R_{avg}}^{1.521}) \tag{12}$$

For $U_t = 0.65746A/B$, the complete dissolution time for a single particle, T_R, is that when r=0, then Eq. (12) becomes

$$T_R = -U_t {R_{avg}}^{1.521} \tag{13}$$

The conversion degree, X, for a single spherical particle is given by

$$1 - X = \frac{(4/3)\pi r^3}{(4/3)\pi R^3} = \left(\frac{r}{R}\right)^3 \tag{14}$$

For particles of common radius R entering reactor j, the degree of conversion is given by

$$\overline{X}_j(R) = 1 - \int_0^\infty (1 - X) E_j(t)\, dt = 1 - \int_0^{T_R} \left(\frac{r}{R}\right)^3 E_j(t)\, dt \tag{15}$$

By considering the size distribution of the feed, $f_{j-1}(R)$, the actual degree of conversion in reactor j is given by

$$\overline{\overline{X}}_j = 1 - \int_0^{R_{max}} f_{j-1}(R) \left\{\int_0^{T_R} \left(\frac{r}{R}\right)^3 E_j(t)\, dt\right\} dR \tag{16}$$

The input size distribution function, $f_0(R)$, can be approximated by a Dawson integral of the form [8]

$$f_0(R) = e^{-R^\beta} \int_{R_{min}}^{R} e^{t^\beta}\, dt \tag{17}$$

The exponent β is a constant characteristic of particle size distribution (β in this work is assumed to be equal to unity). R_{min} and R_{max} (the minimum and maximum radii of the particles) are to be evaluated from the size distribution of the actual feed. Substituting for t and dt from Eq. (8) into Eq. (17) and integrating with respect to r gives

$$f_0(R) = e^{-R}[1 - \exp(U_t({R_{min}}^{1.521} - R^{1.521}))] \tag{18}$$

Substituting for t from Eq. (12) into Eq. (4) gives

$$E_j(t) = \frac{1}{t_{avg}} \exp\left(-U_t \frac{r^{1.521} - R^{1.521}}{t_{avg}}\right) \tag{19}$$

Substituting Eqs. (18) and (19) into Eq. (16) gives

$$\overline{\overline{X}}_j = 1 - \left[\int_0^{R_{max}} e^{-R}\{1 - \exp(U_t({R_{min}}^{1.521} - R^{1.521}))\} \int_R^0 \frac{1.521 U_t}{t_{avg}} \left(\frac{r}{R}\right)^3 r^{0.521} \exp\left(\frac{-U_t(r^{1.521} - R^{1.521})}{t_{avg}}\right) dr\, dR\right] \tag{20}$$

After evaluating the second integral, Eq. (20) becomes

$$\overline{\overline{X}}_j = 1 - \left[\int_0^{R_{max}} \frac{e^{-R}}{R^3}\{1 - \exp(U_t({R_{min}}^{1.521} - R^{1.521}))\} \times \left\{R^3 + \frac{3.521 R^{1.479}}{1.521a} + \frac{7.042}{(1.521a)^2}(1 - \exp(aR^{1.521}))\right\} dR\right] \tag{21}$$

where $a = U_t/t_{avg}$. This integral has been evaluated numerically using Simpson's $\frac{1}{3}$ rule. It can be seen that the above integral cannot be evaluated at $R = 0$, so it has been evaluated from some very small fraction of $R_{min}(1.5 \times 10^{-6})$ to R_{max}. It has been also noticed that the value of the lower limit of the integral affects, to some extent, the calculated value of the conversion.

2.2.2. Crystallization mechanism

The crystallization process is usually divided into nucleation and crystal growth mechanism [8]. The actual process of nucleation is still uncertain; many mechanisms have been postulated according to the physicochemical steps involved in the nuclei formation. Roughly, one can assume both a heterogeneous and a homogeneous mechanism for nuclei formation. The relative importance of these nuclei sources is strongly dependent on the system under examination and must be determined experimentally for each case.

The experimental work of Amin and Larson [11] concerning just the dissolution of phosphorites and $CaSO_4 \cdot \frac{1}{2}H_2O$ crystallization gives information on nucleation rate for this system. These authors indicate that the predominant source of nuclei is homogeneous nucleation and the nuclei generation rate is not dependent on solid present, but only on supersaturation.

The process of crystal growth has been studied extensively and many mechanisms have been postulated. Basically, all these mechanisms involve the following two steps in series [8]: (a) diffusion of crystallizing compound from the bulk solution to the crystal surface, and (b) integration of the above compound in the crystal lattice. Both steps depend on the value of the supersaturation. Shakourzadeh et al. [7] stated that as the phosphate rock dissolves in the reactor, supersaturation of calcium sulfate occurs, leading to gypsum crystallization which involves both nucleation and crystal growth.

The crystal growth rate, υ_e, is given by

$$\upsilon_e = K_L S \tag{22}$$

where S is the supersaturation of calcium sulfate defined by

$$S = C_{CS}(j) - C_{CS}{}^*(j) \tag{23}$$

where $C_{CS}(j)$ and $C_{CS}{}^*(j)$ are, respectively, the supersaturation and equilibrium concentrations of calcium sulfate in reactor j. Based on previous works, Gioia et al. [8] give the following correlation for the equilibrium concentration (solubility) of $CaSO_4$ in solution:

$$C_{CS}{}^*(j) = \rho(7.27 \times 10^{-5}T + 0.024) - 3.46 \times 10^{-2}C_{PA}(j) \tag{24}$$

where C_{PA} is the concentration of H_3PO_4 in the reactor and T the reactor temperature (°C). The linear crystal growth rate υ_L (m/h) is given by [8]

$$\upsilon_L = \frac{dL}{dt} = \left(\frac{K_L M_{G2}}{\rho_{G2} M_G}\right) S = KS \tag{25}$$

where L is the characteristic dimension of the crystal (m), M_G, M_{G2} the molecular weights of $CaSO_4$ and $CaSO_4{\cdot}2H_2O$, respectively (kg/kmol), ρ_{G2} the density of produced gypsum crystals (kg/m^3), and K the constant in the linear crystal growth rate (m^4/h kg).

The crystal population density in reactor j, ψ_j (#/kg m), is given by

$$\psi_j = \psi_{j-1} + (\psi_j{}^0 - \psi_{j-1})\exp\left(\frac{-L}{\upsilon_L t_{avg}}\right) \tag{26}$$

where $\psi_j{}^0$ is the nuclei population density in reactor j (#/kg m) and is given by [8]

$$\psi_j{}^0 = 2.15 \times 10^{19}(\upsilon_L)^{1.6} \tag{27}$$

Similar correlation but with different parameters is also given by Shakourzadeh et al. [7]. For the first reactor Eq. (26) has the form

$$\psi_1 = \psi_1{}^0 \exp\left(\frac{-L}{\upsilon_L t_{avg}}\right) \tag{28}$$

Lastly, the mass fraction of gypsum per unit mass of slurry in reactor j, B_j (kg/kg) is given by

$$B_j = \rho_{G2}\,\phi_{G2}\int_0^\infty L^3 \psi_j(L)\,dL \tag{29}$$

After substitution for ψ_j from Eq. (26) and integration of Eq. (29), the mass fraction of gypsum per unit mass of slurry in reactor j is given as

$$B_j = 6\rho_{G2}\,\phi_{G2}\,\psi_j{}^0(\upsilon_L t_{avg})^4 \tag{30}$$

2.3. System parameters

2.3.1. Density and viscosity of the liquid solution

The density and viscosity of the liquid phase in reactor j have been evaluated as a function of temperature and composition by using the implicit relationships reported by Slack [6] and Gioia et al. [8] after some manipulation of the definition of density. No correction for the effect of impurities on these properties is considered here.

$$\rho = \frac{-b \pm (b^2 + 4ac)^{1/2}}{2a} \tag{31}$$

where

$$a = 1.0, \qquad b = -934.4 - 0.08T,$$
$$c = (2T - 1140)C_{PA}(j) + (1.42T - 667.4)C_{CS}(j) + (1.96T - 921.2)C_{SA}(j) \tag{32}$$

$$\mu = 3.6[10^{(0.479-0.0107T)} + 10^{(-1.183+2.66\times10^{-3}T+(3.24-0.013T)C_{PA}(j)/\rho)}] \tag{33}$$

where T is the temperature (°C), $C_{PA}(j)$ the concentration of H_3PO_4 in reactor j (kg/m^3), and $C_{SA}(j)$ the concentration of H_2SO_4 in reactor j (kg/m^3).

2.3.2. Degree of supersaturation

The degree of supersaturation, based on total concentrations in solution, has been defined as the ratio between the product of the concentrations of calcium and sulfate ions in the supersaturated solution to that in the equilibrium solution [10]

$$G = \frac{[Ca^{2+}][SO_4^{2-}]}{[Ca^{2+}]_{eq}[SO_4^{2-}]_{eq}} \quad (34)$$

By assuming Ca^{2+} concentration equal to the SO_4^{2-} concentration, Eq. (34) becomes [8]

$$G = \left(1 + \frac{S}{C_{CS}^*}\right)^2 \quad (35)$$

Other system parameters such as the mass transfer coefficient and the solubility of gypsum in acid solutions are already discussed in Section 2.2.

2.4. Algorithm of solution

The main idea in formulating the program is to make total and component material balances for all components in all vessels (reactors, filter–feed tank and filter). Equations used to calculate the mass flow rates and mass fractions of all streams leaving the pilot plant vessels are all listed in Appendix A. The algorithm of solution of the three-CSTR pilot plant system is schematically shown in Fig. 2.

The program starts by reading input data (Tables 1 and 3) and initial guesses for slurry recycle composition and conversion in each reactor. With these initial guesses, subroutine GAS calculates the gas mass flow rates leaving the reactors and the filter–feed tank, while subroutine PLANT calculates the theoretical mass flow rates and mass fractions of the sulfuric acid required to be fed to Reactor 3, and phosphoric acid and gypsum expected to be produced.

The output mass flow rates and mass fractions of the streams leaving the reactors are calculated by using the corresponding reactors' subroutines shown in Appendix A. The kinetics and crystallization parameters as well as the conversion in each reactor are also calculated for each reactor using the equations presented earlier in Section 2.2. The calculated output mass fractions from Reactor 3 (i.e., slurry recycle composition) are compared with the initial guess composition. If their absolute difference is higher than a specified error tolerance, ε, then the new composition values are taken as a new guess, and the next trial of calculations proceeds in the same sequence mentioned above. When the absolute difference between successive values (of all compositions leaving Reactor 3) is less than ε, the filter–feed tank output mass flow rate and mass fractions are calculated using the Filter–feed Tank subroutine. Lastly, the mass flow rates and mass fractions of the phosphoric acid product and gyp-

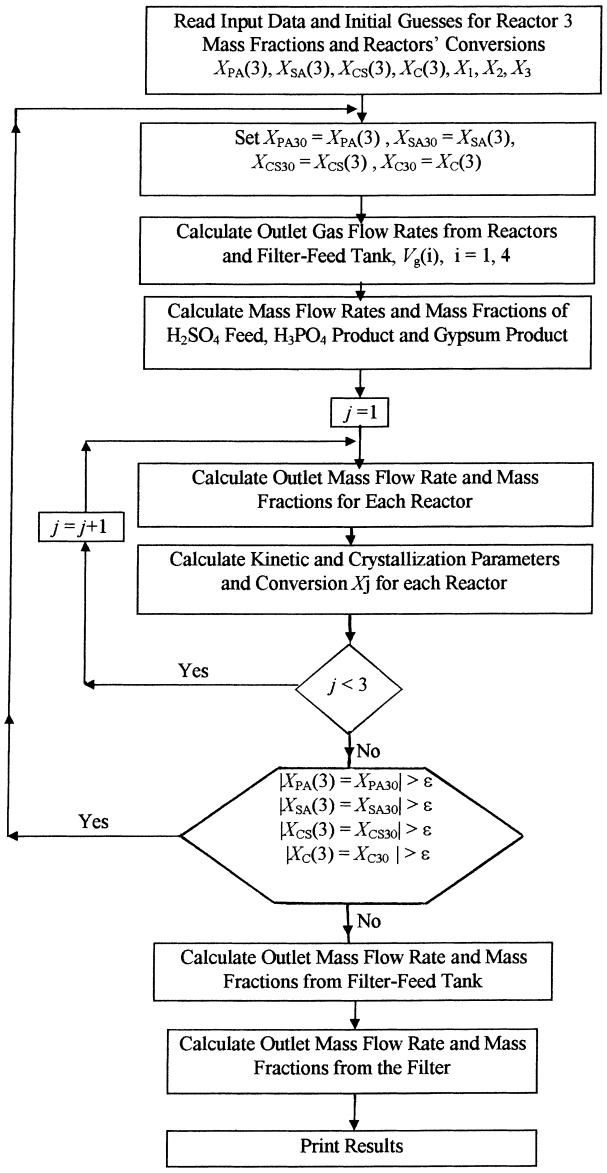

Fig. 2. Schematic diagram for the procedure of calculation followed in this work.

Table 1
Phosphate rock chemical analysis

Component	Wt.%
P_2O_5	32.28
CaO	50.91
CO_2	5.20
SiO_2	4.47
F	3.64
SO_4^{2-}	1.54
MgO	0.27
Al_2O_3	0.42
Fe_2O_3	0.23
Na_2O	0.59
K_2O	0.04
Cl	0.045
Organic matter	0.12
Combined water	0.76

Table 2
Phosphate rock screen analysis

Sieve size (mesh)		Aperture (μm)		Wt.%
−30	+60	−500	+250	0.55
−60	+100	−250	+150	21.50
−100	+150	−150	+106	23.60
−150	+200	−106	+75	10.30
−200		−75		44.05

sum byproduct leaving the filter are calculated using Filter subroutine.

3. Analysis of results and discussion

3.1. Input data

In the JPMC pilot plant experiments, two samples of dry phosphate fines collected from cyclones during drying of the phosphate grades were received from El-Abiad phosphate mine. The two samples were blended together to form "Abiad Blend No. 1". The chemical and screen analysis of the blend are shown in Tables 1 and 2. According to JPMC, the size analysis of the blend is suitable for the dihydrate process [5]. Design and actual operating conditions of the JPMC pilot plant are shown in Table 3 where each stream flow rate, composition and density are listed. Some of the physical properties such as particles size, phosphate rock density, and sulfuric acid, return acid and slurry recycle densities have been taken from the JPMC pilot plant records for this specific work. The shape factor has been arbitrarily taken as unity assuming spherical shape particles. The value of the diffusivity coefficient of H^+ ions in the solution (1.1×10^{-6} m^2/h) has been taken from [14].

Table 3
JPMC pilot plant operating conditions and other data

Stream	Value
Phosphate rock feed to Reactor 1	
Flow rate, F_F (kg/h)	10.0
Minimum particle size, R_{min} (m)	1.5×10^{-5}
Average particle size, R_{avg} (m)	5.0×10^{-5}
Maximum particle size, R_{max} (m)	12.0×10^{-5}
Mineral density, ρ_M (kg/m^3)	2200
Shape factor, Φ_M	1.0
Sulfuric acid to mixing box	
Flow rate, F_A (kg/h)	9.053
Concentration, C_{SA} (wt.%)	98.0
Density (kg/m^3)	1840
Reactors	
Reaction volume/tank, V (m^3)	0.0515
Reactor diameter, D_T (m)	0.415
Impeller diameter, D_I (m)	0.10
Impeller speed, ω (rph)	7800
Temperature (°C)	80
Diffusivity coefficient, D_v (m^2/h) assumed	1.1×10^{-6}
Return acid from filter to mixing box	
Flow rate, F_R (kg/h)	24.2
P_2O_5 concentration, C_{PR} (wt.%)	18.4
Density (kg/m^3)	1179
Wash water flow rate, F_W (kg/h)	11.2
Makeup water flow rate, F_V (kg/h)	0.0
Slurry recycle from Reactor 3 to Reactor 1	
Flow rate, F_{RS} (kg/h)	822.28
Density (kg/m^3)	1550

Table 4
Comparison between model results and JPMC pilot plant actual results, as applied to Reactor 3 using the operating conditions listed in Table 3

Quantity	JPMC value	Model value	Relative error (%)
H_3PO_4 mass fraction	0.4095	0.40113	2.04
H_2SO_4 mass fraction	0.0355	0.03427	3.46
$CaSO_4$ mass fraction	0.2881	0.29810	3.47
CaO mass fraction	0.0050	0.00504	0.80
H_2SO_4 feed rate (kg/h)	9.053	9.091	0.42
Conversion, X_3	97.5	95.47	2.08

As a first approximation, the amount of sulfuric acid required for acidulation has been equated to that required to combine with all calcium ions present in the phosphate rock to form calcium sulfate. This calculated value is often close enough for planning purposes [12]. Table 4 shows some model-predicted results vs. JPMC experimental data. It is clear that the predicted values are close enough to the experimental data and the absolute relative error range is 0.42–3.5%.

The parametric study carried out in this work using the JPMC pilot plant mathematical model and presented below, covers the effect of reaction temperature, sulfuric acid feed flow rate, agitator–impeller speed, and slurry recycle and return acid flow rates (or their ratios to the feed rate). A schematic diagram of the calculation procedure is shown in Fig. 2. The main equations used to calculate the effect of the above-mentioned parameters on the system performance are listed in Table 5.

Table 5
Main equations used to study the phosphoric acid pilot plant performance

Parameter value in reactor j	Equation used
Mean residence time, t_{avg}	Eq. (5)
Dissolution rate of a single particle, υ_M	Eq. (7)
Mass transfer coefficient, K_L	Eq. (11)
Complete dissolution time of a single particle, T_R	Eq. (13)
Overall conversion, X_j	Eq. (21)
Crystal growth rate, υ_e	Eq. (22)
Supersaturation, S	Eq. (23)
Calcium sulfate equilibrium concentration, $C_{CS}{}^*$	Eq. (24)
Linear crystal growth rate, υ_L	Eq. (25)
Crystal population density, ψ_j	Eq. (26)
Nuclei population density, $\psi_j{}^0$	Eq. (27)
Mass fraction of gypsum per unit mass of slurry, B_j	Eq. (30)
Degree of supersaturation, G	Eq. (35)

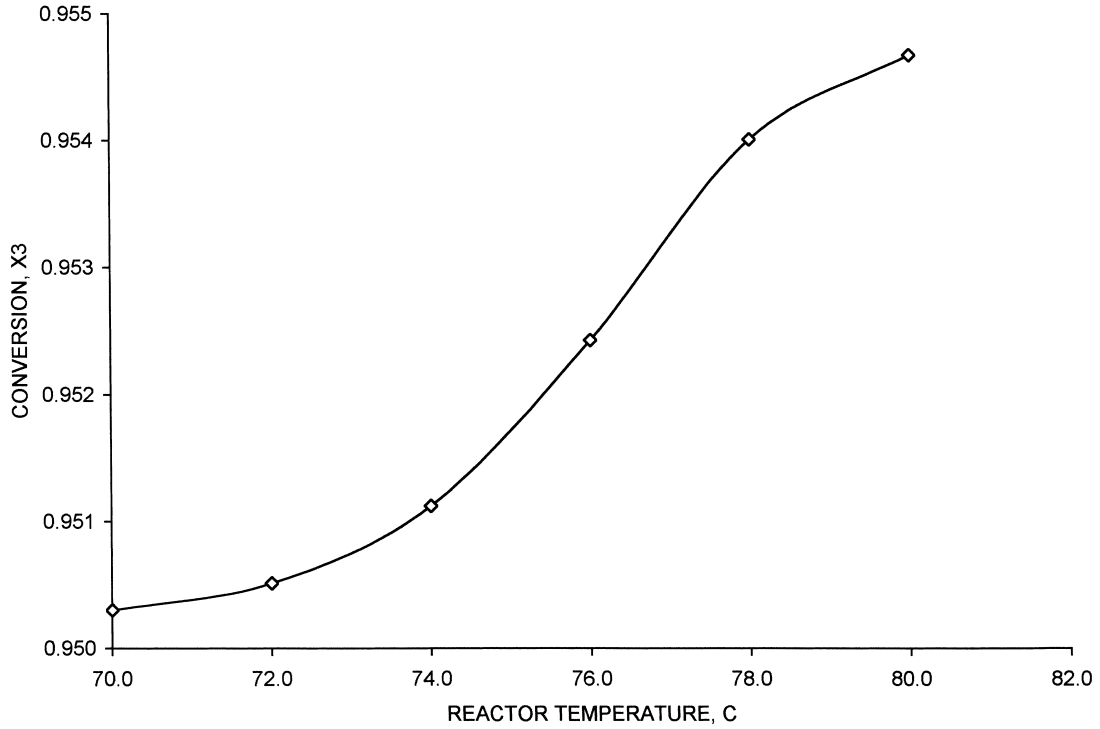

Fig. 3. Overall conversion in Reactor 3 vs. temperature (see Table 3 for other operating conditions).

3.2. Effect of reaction temperature

The temperature range of 70–80°C has been considered here, since as mentioned earlier, the calcium sulfate crystallizes in the dihydrate form in this range. As shown in Fig. 3, the overall conversion of the process, represented by conversion in Reactor 3, only slightly increases with the increase in temperature, but as shown in Fig. 4, the effect of tempe-

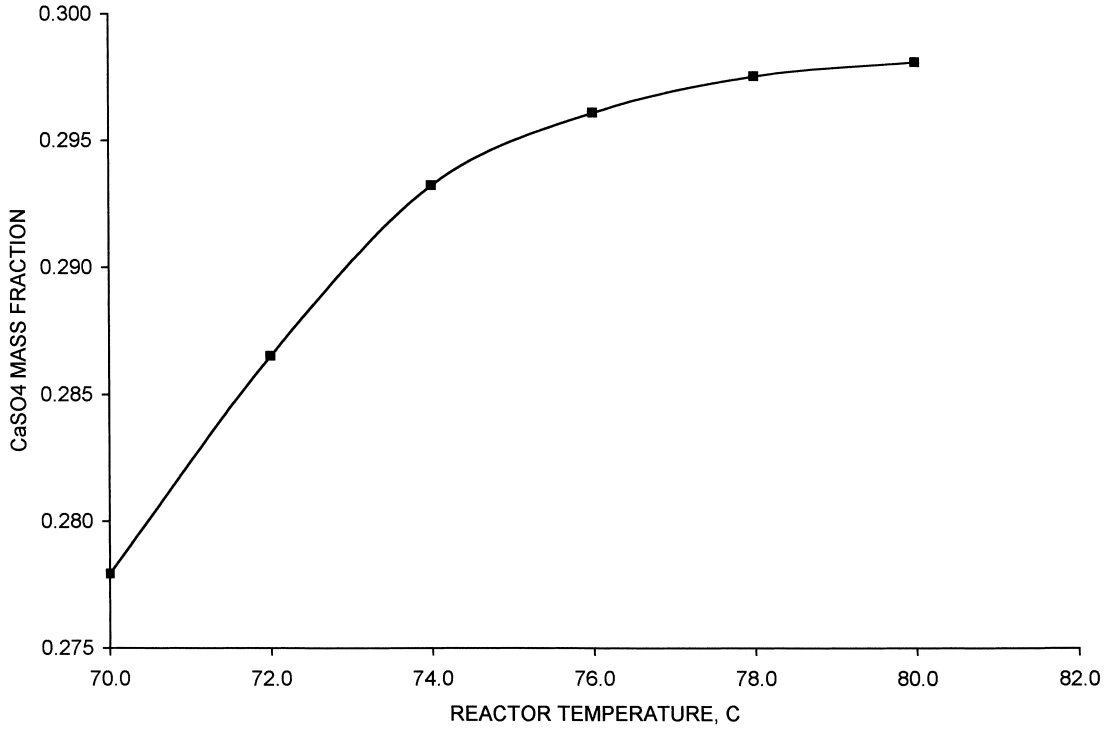

Fig. 4. $CaSO_4$ mass fraction in Reactor 3 vs. temperature (see Table 3 for other operating conditions).

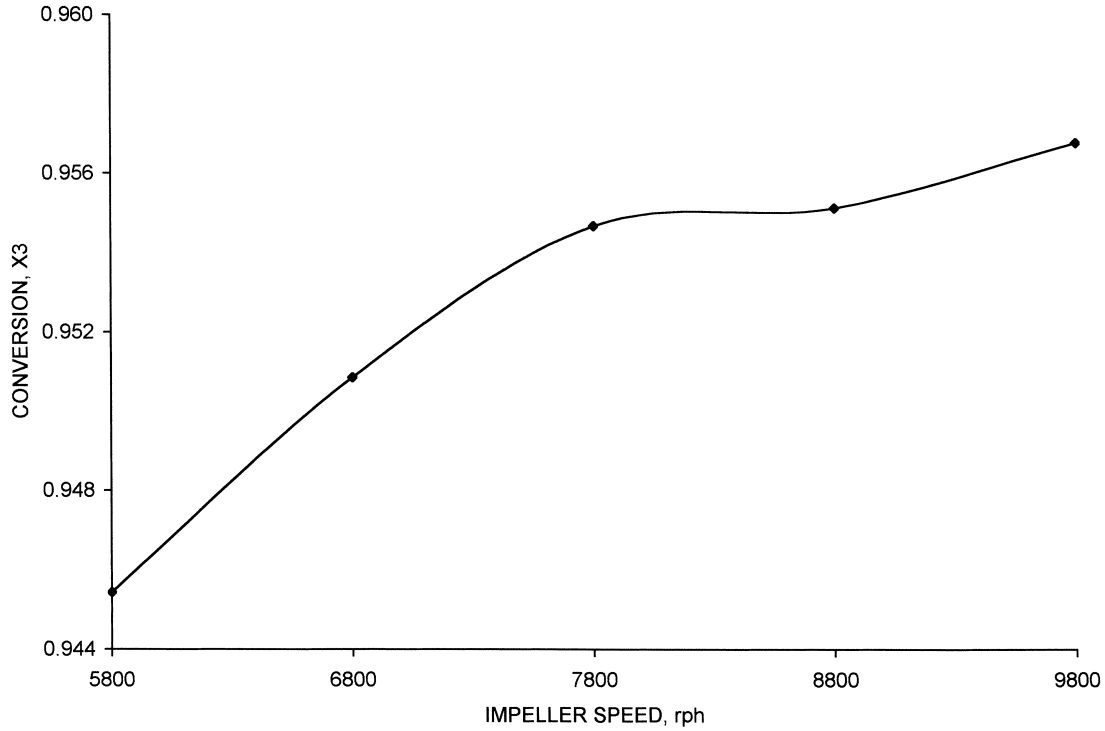

Fig. 5. Overall conversion in Reactor 3 vs. impeller speed (see Table 3 for other operating conditions).

rature on calcium sulfate formation in Reactor 3 is more pronounced, the rate of formation of calcium sulfate start high then reaches a steady value as temperature increases. This is probably due to the fact that a calcium sulfate layer formed on the outer surface of the phosphate particles hinders the rate of reaction.

3.3. Effect of sulfuric acid feed rate

As expected, increasing sulfuric acid feed rate causes some increase in its concentration in the reactor and in the slurry recycle stream. It has been found that increasing sulfuric acid feed rate from 9.1 to 10.0 kg/h had caused only a slight increase in its concentration in Reactor 3 (from 52.3 to 53.8 kg/m^3). This in turn caused a slight increase in the dissolution rate of the rock in Reactor 3 (from 5.60 to 5.77 kg/h m^2) and conversion (from 95.46 to 95.58%), and a slight decrease in the dissolution time of single phosphate rock particles. Based on these facts, the optimum flow rate of sulfuric acid feed is determined only from its cost and pumping requirements in the plant.

On the other hand, the presence of sulfuric acid, in general, reduces the solubility of the calcium sulfate crystals due to the common ion effect. Also the presence of excess sulfuric acid increases the pH of the solution, which may increase the solubility of calcium sulfate [15].

3.4. Effect of agitator–impeller speed

It is expected that by increasing the agitator–impeller speed the dense layer coating the phosphate rock core to break down and it will be removed by the reaction solution. This will give the phosphate core further chance to react and cause the rate of reaction as well as the overall conversion to increase. Upon increasing the impeller speed from 5000 to 10 000 rph, the dissolution rate of the phosphate rock in Reactor 3, e.g., has increased from about 4.6–5.9 kg/h m^2 and X_3 increased from 94.1 to 95.7% (see Fig. 5). As a result, the complete dissolution time of a single phosphate particle decreased from 0.84 to 0.66 min when the impeller speed was increased from 5000 to 10 000 rph. On the other hand, increasing the impeller speed will bring the calcium sulfate crystals to collide with each other thus forming larger crystals (i.e., larger linear crystal and crystal growth rates) with higher nuclei population densities (see Table 6).

Table 6
Effect of impeller speed on crystal growth rate and nuclei population density using the operating conditions listed in Table 3

Impeller speed, ω (rph)	Crystal growth rate, υ_e (kg/h m^2)	Nuclei population density, $\psi_j{}^0$ (#/kg m)
5000	40.85	0.956×10^{17}
7800	46.43	1.169×10^{17}
10000	52.45	1.426×10^{17}

Based on the above results, one might think of running the reactors at higher impeller speeds. However, this is not recommended because increasing the crystal growth rate to a higher limit will make filtration harder and consumes a lot of power. Also filtration rate decreases with the increase of nucleation rate [4].

3.5. Effects of slurry recycle flow rate

Upon increasing the slurry recycle flow rate, F_{RS}, it has been noticed that the overall conversion, phosphoric acid concentration and dissolution rate of a single phosphate particle all increase until they reach some upper limit, after which the dense calcium sulfate layer probably coats the phosphate rock core thus preventing the acid solution from reaching the core surface (see Figs. 6–8). Such coating is often referred to as blinding [9,10].

For example, Fig. 6 shows that, upon increasing F_{RS} from 400 to 1200 kg/h, the conversion in Reactor 3, X_3, reaches a maximum (at F_{RS}=822 kg/h), after which it becomes almost steady at 95.4%. Fig. 7 shows that the H_3PO_4 concentrations in Reactors 1 and 3 increase sharply until they reach some maximum (at F_{RS}=822 kg/h), after which it again becomes almost steady. Fig. 7 also shows that the H_3PO_4 concentration in Reactor 1 is a little higher than that in Reactor 3. Lastly, Fig. 8 shows that the dissolution rate of the phosphate rock in Reactor 3 is much steadier and higher in Reactor 3 than in Reactor 1.

The effect of slurry recycle on the complete dissolution time of a single phosphate particle in Reactors 1 and 3 is shown in Fig. 9. It is clear that this dissolution time is sharply decreasing for Reactor 1 and almost constant for Reactor 3, and it becomes almost constant at higher slurry recycle flow rates of about 700 kg/h and above. On the other hand, Fig. 10 shows that the degree of supersaturation (defined by Eq. (35)), which is affected by temperature and acid concentrations in the reactors [15], slowly increases at low slurry recycle flow rates (below F_{RS}=822 kg/h) and sharply increases for F_{RS} above 822 kg/h.

3.6. Effect of return acid flow rate

The return acid from the filter, whose composition is mainly phosphoric acid (about 18.4% P_2O_5), is very important for the initiation of the reaction. It reacts with the phosphate rock to form a soluble monocalcium phosphate compound which in turn reacts with sulfuric acid to form phosphoric acid and calcium sulfate. Thus, it is expected that by increasing the return acid flow rate, the reaction rate will increase until it reaches a maximum, beyond which rock blinding occurs and the particles are prevented from further reaction with the acid solution.

This is exactly what has been noticed upon increasing the return acid flow rate, F_{RA}, from 12 to 36 kg/h, where a flat maximum in conversion in Reactor 3 has been obtained, as shown in Fig. 11 (at F_{RA} between 24 and 32 kg/h). The same is true for the dissolution rate of the phosphate rock as shown in Fig. 12. This also justifies the results shown in Fig. 13 where the complete dissolution time of a single particle has a flat minimum for the same return acid flow rate range.

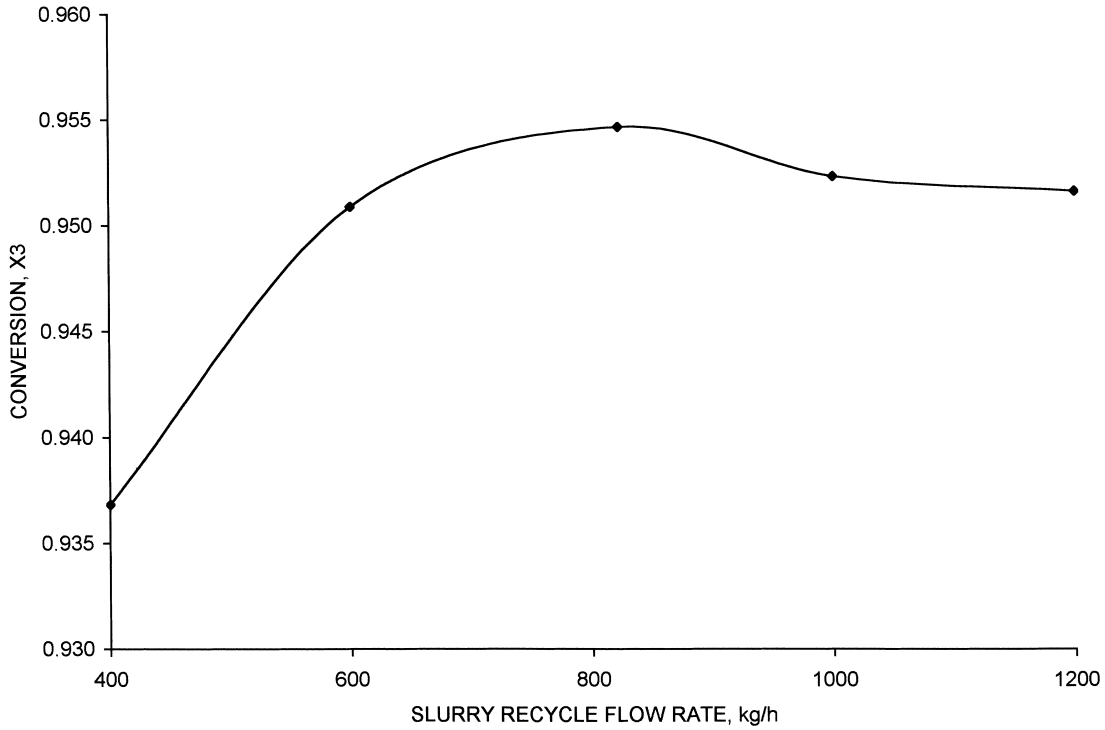

Fig. 6. Overall conversion in Reactor 3 vs. slurry recycle flow rate (see Table 3 for other operating conditions).

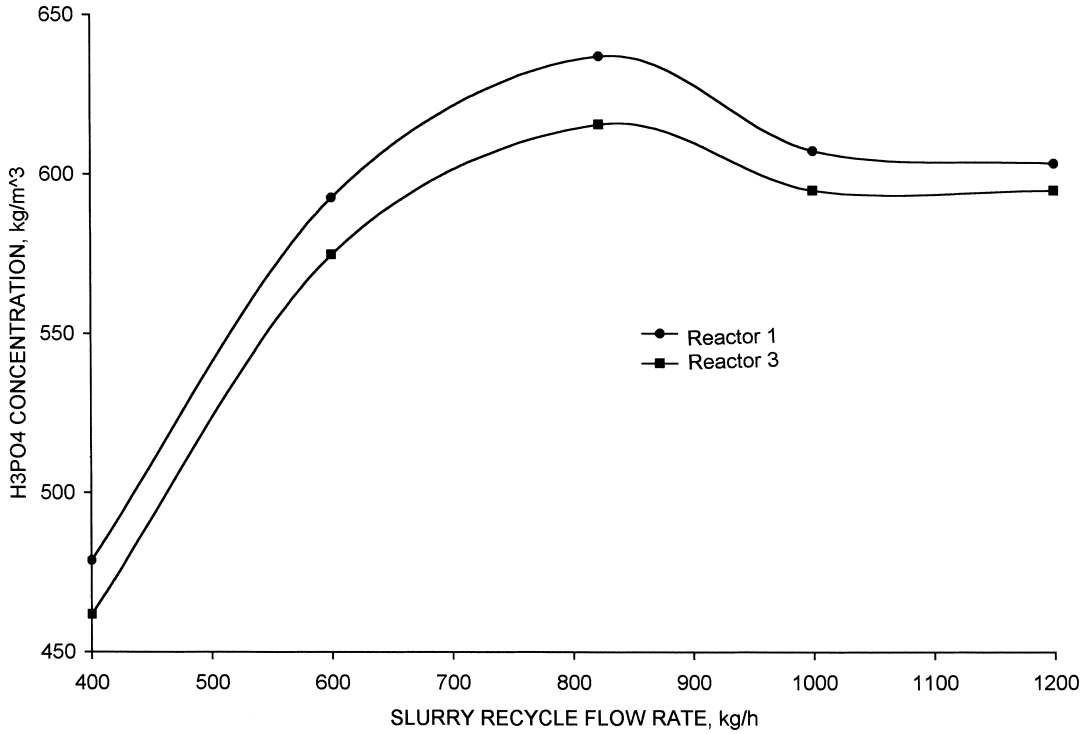

Fig. 7. H_3PO_4 concentration in Reactors 1 and 3 vs. slurry recycle flow rate (see Table 3 for other operating conditions).

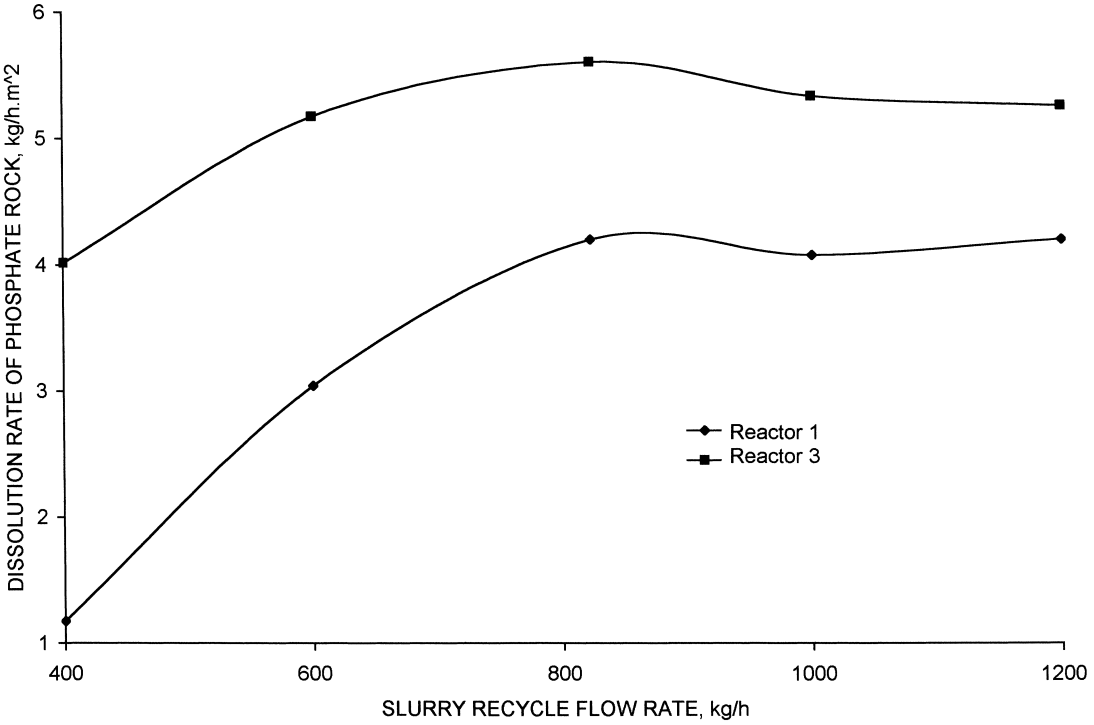

Fig. 8. Phosphate rock dissolution rate in Reactors 1 and 3 vs. slurry recycle flow rate (see Table 3 for other operating conditions).

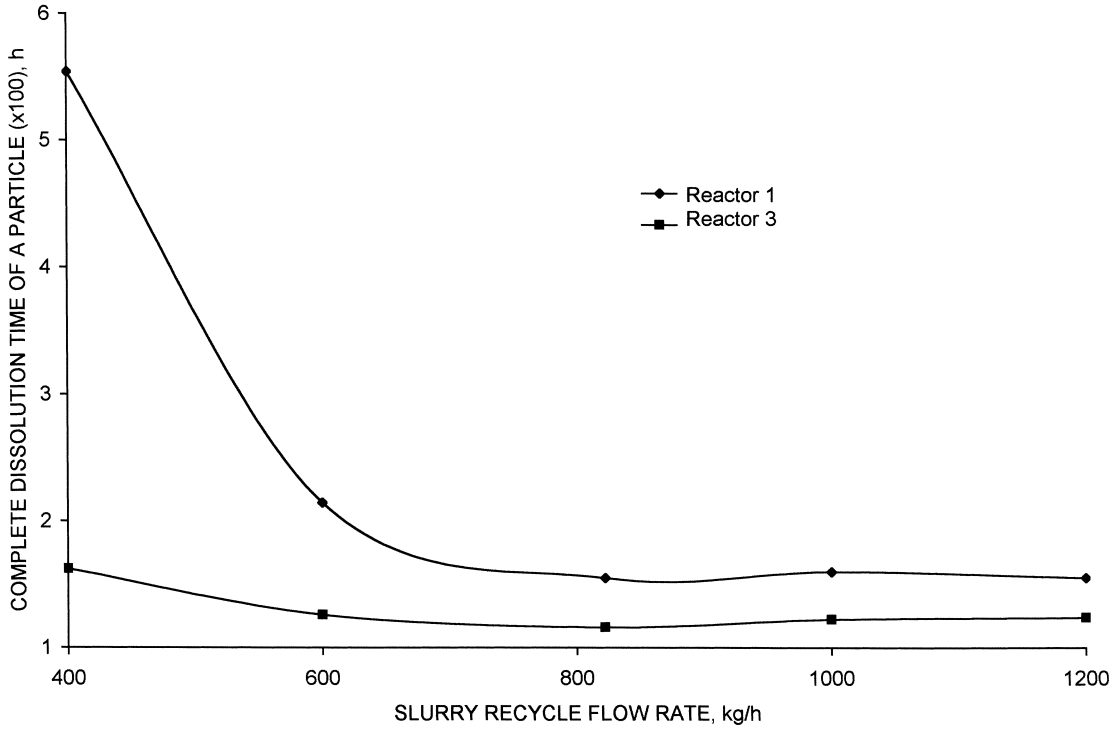

Fig. 9. Complete dissolution time of a single particle in Reactors 1 and 3 vs. slurry recycle flow rate (see Table 3 for other operating conditions).

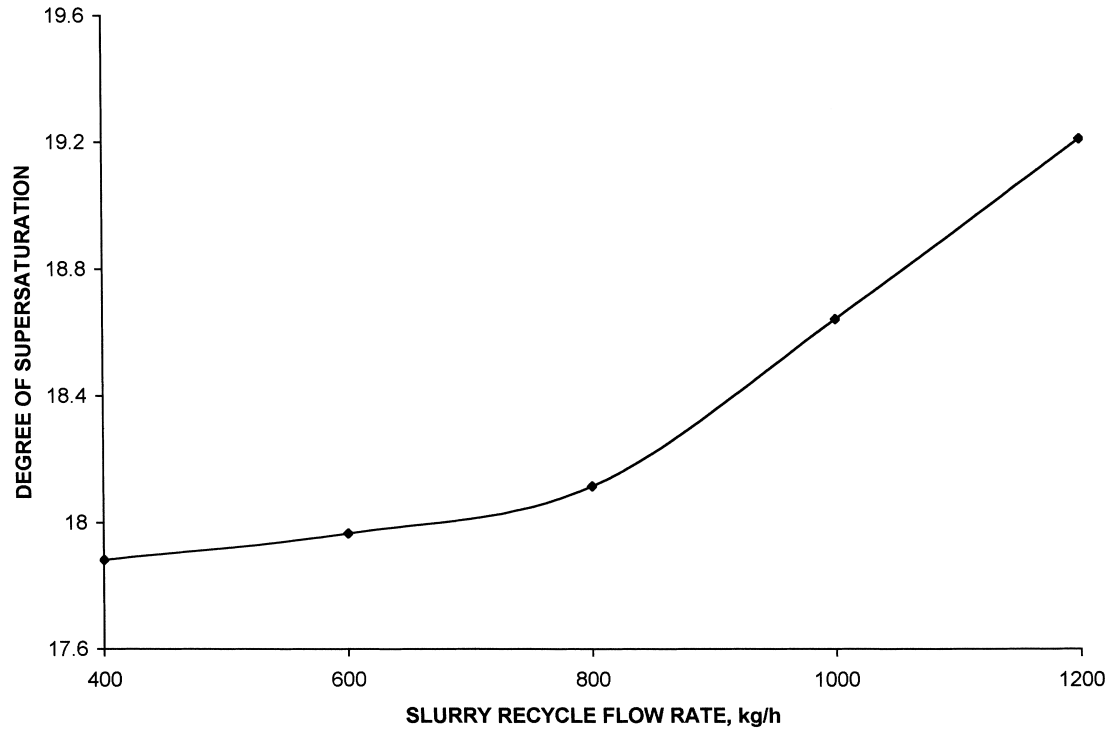

Fig. 10. Degree of supersaturation in Reactor 3 vs. slurry recycle flow rate (see Table 3 for other operating conditions).

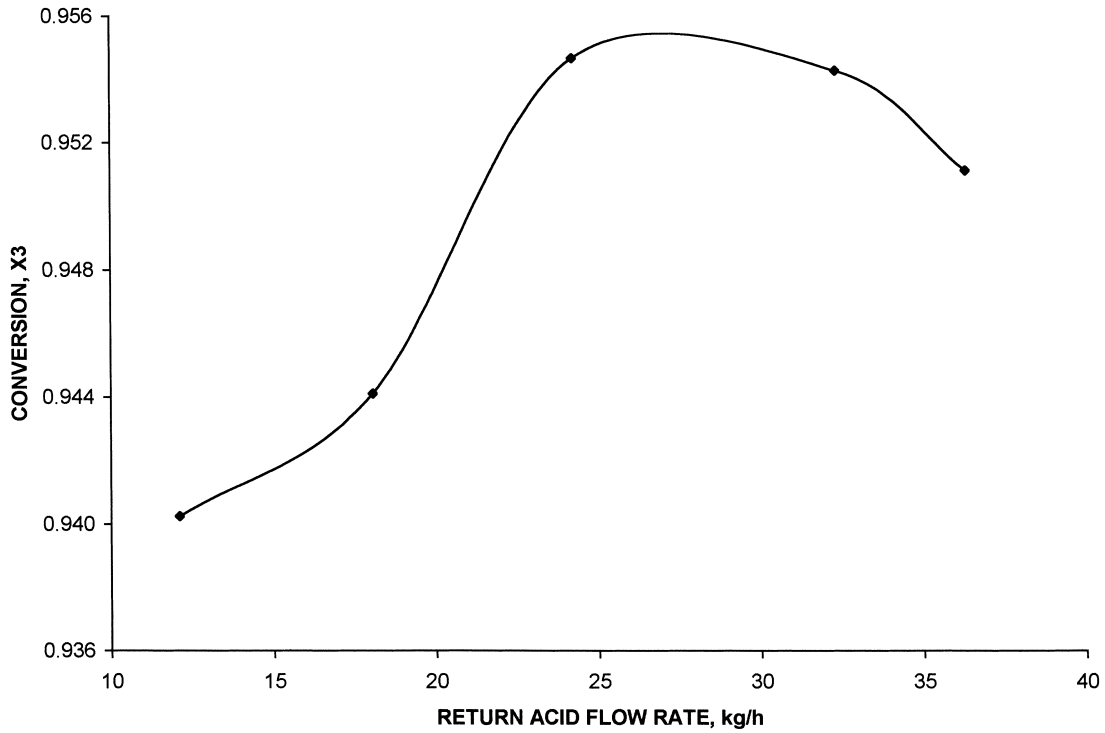

Fig. 11. Overall conversion in Reactor 3 vs. return acid flow rate (see Table 3 for other operating conditions).

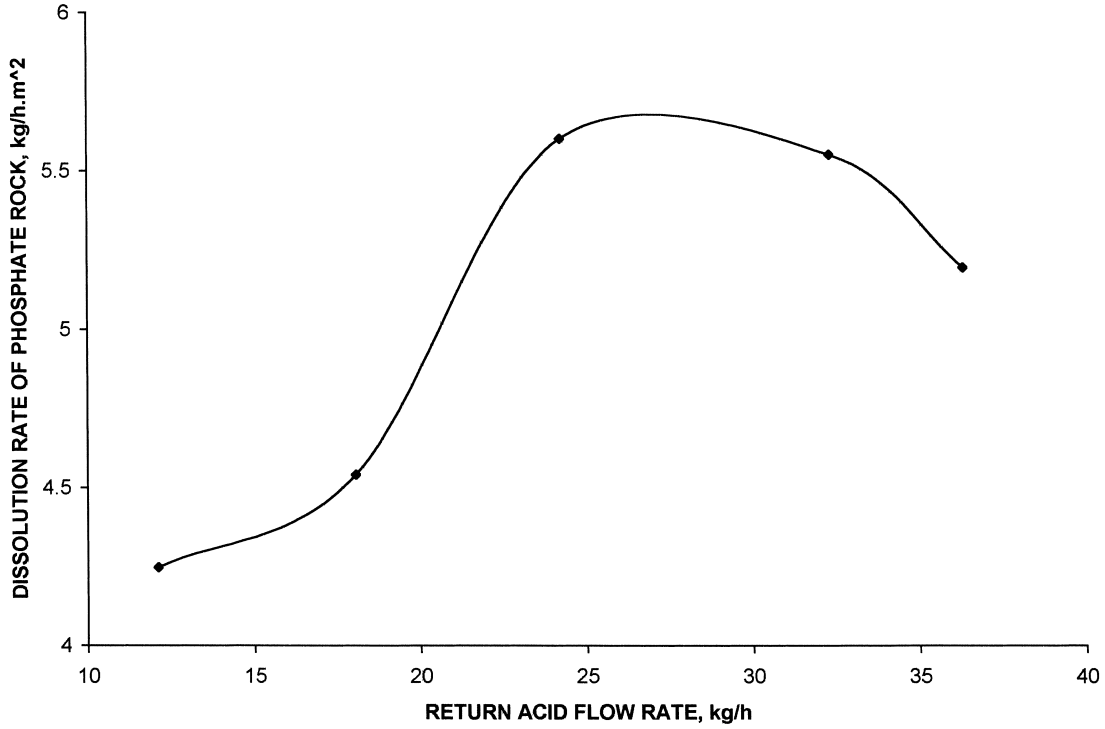

Fig. 12. Phosphate rock dissolution rate in Reactor 3 vs. return acid flow rate (see Table 3 for other operating conditions).

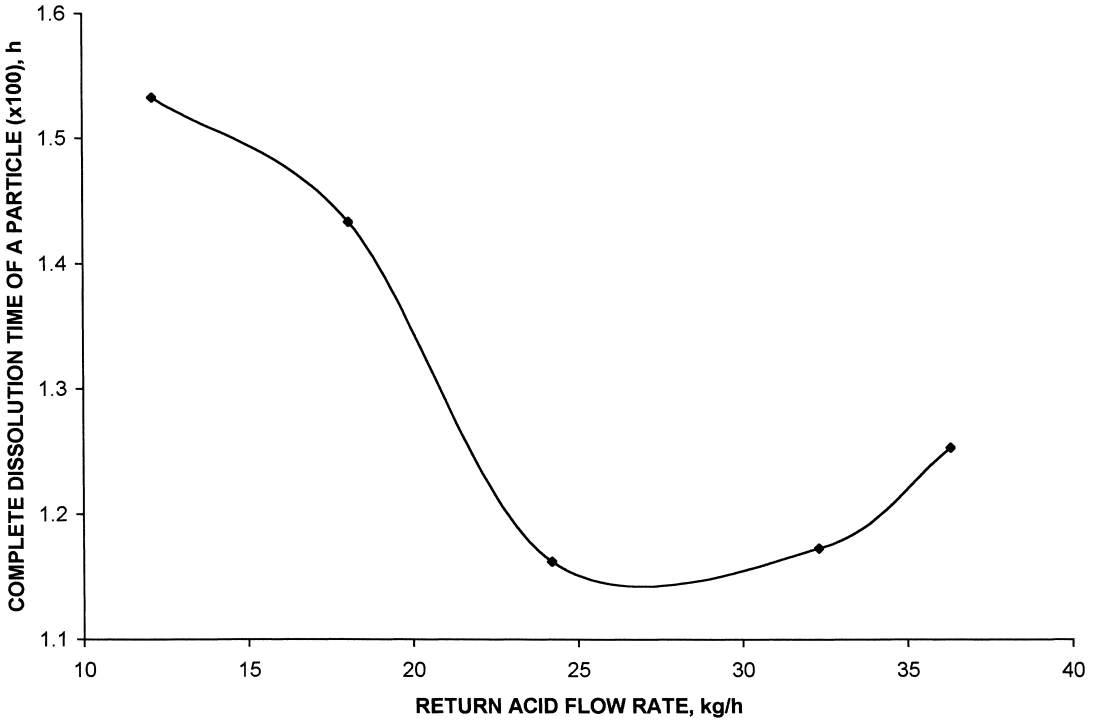

Fig. 13. Complete dissolution time of a single phosphate particle in Reactor 3 vs. return acid flow rate (see Table 3 for other operating conditions).

4. Conclusions and recommendations

Simulation modeling of the production of phosphoric acid by the dihydrate process has been used in this work as an illustration of the application of the principles of chemical engineering to the analysis of real processes. Solving this simulation model has showed that, the knowledge of these principles is sufficient to get a reasonable description of what is going on in the "real life" process. Such work is very important in saving time and effort required for conducting pilot plant or industrial plant experiments.

The results of the simulated model have been found to represent the behavior of the process in a very good manner, with an absolute relative error of less than 3.5% from real pilot plant results. The authors believe that, with some modifications, the above model can be easily extended to simulate actual situations in industrial phosphoric acid plants.

For the specific feed studied in this work, a reactor temperature of 80°C, a slurry recycle to feed ratio of 80, and a return acid to feed ratio of 2.5 have been found to give best results. The optimum conditions for sulfuric acid feed rate and agitation speed as operating parameters, are determined only from power limitations and the economics of the plant itself.

Since this study focuses on pilot plant's performance, it is recommended to extend application of this model to industrial plants. It is also recommended to study the effect of phosphate rock impurities and size distribution on the process performance. The effect of initial size of phosphate rock particles on coating is not considered in this work and it might worth investigation in a future work.

Appendix A. Summary of the model material balance equations

A.1. GAS subroutine

Total mass flow rate of HF produced:

$$m_{HF,T} = F_F X_{FF} M_{HF}/M_F$$

Mass flow rate of HF released as a gas from all vessels (0.4 is assumed):

$$m_{HF,V} = 0.4 m_{HF,T}$$

Mass flow rate of HF converted to H_2SiF_6 in the liquid phase (0.6 is assumed):

$$m_{HF,L} = 0.6 m_{HF,T}$$

Mass flow rate of CO_2 produced from carbonates and organic matter entering with the feed:

$$m_{CO_2} = F_F(X_{CO_2} + X_{ORG})$$

Total mass flow rate of gases released from all vessels:

$$V_T = m_{HF,V} + m_{CO_2}$$

Mass flow rate of gases released from vessels 1–4:

$$V_g(1) = X_1 V_T,$$
$$V_g(2) = (X_2 - X_1)(V_T - V_g(1)),$$
$$V_g(3) = (X_3 - X_2)[V_T - V_g(1) - V_g(2)],$$
$$V_g(4) = V_T - V_g(1) - V_g(2) - V_g(3)$$

A.2. PLANT subroutine

Mass fraction of SO_4 in H_2SO_4 feed:

$$X_S = X_A M_S / M_{SA}$$

Theoretical mass flow rate of H_2SO_4 required:

$$F_A = (F_F X_{CF} M_{SA} / M_C) / X_A$$

Theoretical mass flow rate of gypsum produced:

$$F_G = F_F X_{CF} M_{G2} / M_C$$

Mass flow rate of H_3PO_4 produced (from overall material balance):

$$F_P = F_F + F_A + F_V + F_W - F_G - V_T$$

Theoretical mass flow rate of 100% H_3PO_4 produced:

$$F_{PA} = (F_F X_{PF} - F_G X_{PG}) 2M_{PA} / M_P$$

Mass fractions of CaO in phosphogypsum:

$$X_{CG} = (F_F X_{CF} - F_P X_{CP}) / F_G$$

Mass fractions of SO_4 in phosphogypsum:

$$X_{SG} = (F_F X_{SF} + F_A X_S - F_P X_{SP}) / F_G$$

A.3. REACTOR 1 subroutine

Total volumetric flow rate entering Reactor 1:

$$Q_1 = F_F / \rho_M + F_{RS} / \rho_3$$

Concentration of H_3PO_4 in Reactor 1:

$$C_{PA}(1) = [F_{RS} X_{PA}(3) + X_1 F_F X_{PF}\, 2M_{PA} / M_P] / Q_1$$

Concentration of H_2SO_4 in Reactor 1:

$$C_{SA}(1) = [F_{RS} X_{SA}(3) - X_1 F_F X_{CF} M_{SA} / M_C] / Q_1$$

Concentration of $CaSO_4$ in Reactor 1:

$$C_{CS}(1) = [(F_F X_1((X_{CF} - X_{SF}) M_C / M_S) M_G / M_C) + F_{RS} X_{CS3} + (F_F X_{SF} M_G / M_S) + X_1 F_{RS} X_C(3) M_G / M_C] / Q_1$$

Outlet mass flow rate from Reactor 1:

$$F(1) = F_F + F_{RS} - V_g(1)$$

Mass fraction of H_3PO_4 in F(l):

$$X_{PA}(1) = [(X_1 F_F X_{PF}\, 2M_{PA} / M_P) + F_{RS} X_{PA}(3)] / F(1)$$

Mass fraction of remained unconverted P_2O_5 in F(1):

$$X_P(1) = F_F X_{PF}(1 - X_1) / F(1)$$

Mass fraction of remained unconverted CaO in F(1):

$$X_C(1) = [(1 - X_1) F_F((X_{CF} - X_{SF}) M_C / M_S) + F_{RS} X_C(3)] / F(1)$$

Mass fraction of H_2SO_4 in F(1):

$$X_{SA}(1) = [F_{RS} X_{SA}(3) - X_1 F_F X_{CF} M_{SA} / M_C] / F(1)$$

Mass fraction of $CaSO_4$ in F(1):

$$X_{CS}(1) = [(F_F X_{SF} M_G / M_S) + (F_F X_1 (X_{CF} - X_{SF} M_C / M_S) M_G / M_C) + (X_1 F_{RS} X_C(3) M_G / M_C) + F_{RS}(3)] / F(1)$$

A.4. REACTOR 2 subroutine

Total volumetric flow rate entering Reactor 2:

$$Q_2 = F_1 / \rho_1$$

Concentration of H_3PO_4 in Reactor 2:

$$C_{PA}(2) = [F(1) X_{PA}(1) + (X_2 - X_1) X_P(1) F(1)\, 2M_{PA} / M_P] / Q_2$$

Concentration of H_2SO_4 in Reactor 2:

$$C_{SA}(2) = \{F(1) X_{SA}(1) - [(X_2 - X_1) F(1) X_C(1) M_{SA} / M_C]\} / Q_2$$

Concentration of $CaSO_4$ in Reactor 2:

$$C_{CS}(2) = [F(1) X_{CS}(1) + (X_2 - X_1) X_C(1) M_G / M_C] / Q_2$$

Outlet mass flow rate from reactor 2:

$$F(2) = F(1) - V_g(2)$$

Mass fraction of H_3PO_4 in F(2):

$$X_{PA}(2) = [F(1) X_{PA}(1) + (X_2 - X_1) F(1) X_P(1)\, 2M_{PA} / M_P] / F(2)$$

Mass fraction of remained unconverted P_2O_5 in F(2):

$$X_P(2) = [1 - (X_2 - X_1)] F(1) X_P(1) / F(2)$$

Mass fraction of remained unconverted CaO in F(2):

$$X_C(2) = [1 - (X_2 - X_1)] F(1) X_C(1) / F(2)$$

Mass fraction of H_2SO_4 in F(2):

$$X_{SA}(2) = [F(1)X_{SA}(1) - (X_2 - X_1)F(1)X_C(1)M_{SA}/M_C]/F(2)$$

Mass fraction of $CaSO_4$ in $F(2)$:

$$X_{CS}(2) = [F(1)X_{CS}(1) + (X_2 - X_1)F(1)X_C(1)M_G/M_C]/F(2)$$

A.5. REACTOR 3 subroutine

Total volumetric flow rate entering Reactor 3:

$$Q_3 = F_2/\rho_2$$

Concentration of H_3PO_4 in Reactor 3:

$$C_{PA}(3) = \{F(2)X_{PA}(2) + [(X_3 - X_2)F(2)X_P(2) + F_R X_{PR}]2M_{PA}/M_P\}/Q_3$$

Concentration of H_2SO_4 in Reactor 3:

$$C_{SA}(3) = [F(2)X_{SA}(2) + F_A X_A - (X_3 - X_2)F(2)X_C(2)M_{SA}/M_C]/Q_3$$

Concentration of $CaSO_4$ in Reactor 3:

$$C_{CS}(3) = [F(2)X_{CS}(2) + ((X_3 - X_2)F(2)X_C(2)M_G/M_C) + F_R X_{GR}]/Q_3$$

Outlet mass flow rate from Reactor 3:

$$F(3) = F(2) + F_A + F_R - F_{RS} - V_g(3)$$

Mass fraction of H_3PO_4 in $F(3)$:

$$X_{PA}(3) = \{F(2)X_{PA}(2) + (X_3 - X_2)[F(2)X_P(2) + F_R X_{PR}]2M_{PA}/M_P\}/(F(3) + F_{RS})$$

Mass fraction of remained unconverted P_2O_5 in $F(3)$:

$$X_P(3) = [1 - (X_3 - X_2)]F(2)X_P(2)/(F(3) + F_{RS})$$

Mass fraction of remained unconverted CaO in $F(3)$:

$$X_C(3) = [1 - (X_3 - X_2)]F(2)X_C(2)/(F(3) + F_{RS})$$

Mass fraction of H_2SO_4 in $F(3)$:

$$X_{SA}(3) = [F(2)X_{SA}(2) + F_A X_A - (X_3 - X_2) \times F(2)X_C(2)M_{SA}/M_C]/(F(3) + F_{RS})$$

Mass fraction of $CaSO_4$ in $F(3)$:

$$X_{CS}(3) = [F(2)X_{CS}(2) + ((X_3 - X_2)F(2)X_C(2)M_G/M_C) + F_R X_{GR}]/(F(3) + F_{RS})$$

A.6. FILTER–FEED TANK subroutine

Outlet mass flow rate:

$$F(4) = F(3) + F_V - V_g(4)$$

Mass fraction of H_3PO_4 in $F(4)$:

$$X_{PA}(4) = F(3)X_{PA}(3)/F(4)$$

Mass fraction of remained unconverted P_2O_5 in $F(4)$:

$$X_P(4) = F(3)X_P(3)/F(4)$$

Mass fraction of remained unconverted CaO in $F(4)$:

$$X_C(4) = F(3)X_C(3)/F(4)$$

Mass fraction of H_2SO_4 in $F(4)$:

$$X_{SA}(4) = F(3)X_{SA}(3)/F(4)$$

Mass fraction of $CaSO_4$ in $F(4)$:

$$X_{CS}(4) = F(3)X_{CS}(3)/F(4)$$

A.7. FILTER subroutine

Outlet mass flow rate of H_3PO_4 product:

$$F_P = F(4) + F_W - F_G - F_R$$

Mass fraction of H_3PO_4 in F_P:

$$X_{PA}(5) = F(4)X_{PA}(4)/(F_P + F_R)$$

Mass fraction of remained unconverted P_2O_5 in phosphogypsum product:

$$X_{PA}(5) = F(4)X_P(4)/F_G$$

Mass fraction of remained unconverted CaO in phosphogypsum product:

$$X_C(5) = [F(4)X_C(4) - F_P X_{CP}]/F_G$$

Mass fraction of H_2SO_4 lost with H_3PO_4 product:

$$X_{SA}(5) = F(4)X_{SA}(4)/(F_P + F_R)$$

Mass fraction of $CaSO_4$ in phosphogypsum product:

$$X_{CS}(5) = [F(4)X_{CS}(4) - F_R X_{GR}]/F_G$$

References

[1] M. Jansen, A. Waller, J. Verbiest, R.C. van Landschoot, G.M. van Rosmalen, Incorporation of phosphoric acid in calcium sulfate hemihydrate from a phosphoric acid process, Industrial Crystallization, Vol. 84, Elsevier, Amsterdam, 1984, pp. 171–176.
[2] G.T. Austin, Shreve's Chemical Process Industries, 5th Edition, McGraw-Hill, Singapore, 1984.
[3] Anonymous, Phosphoric acid: choosing a process, Fertilizer Int. 269 (1989) 32–35.

[4] S.K. Sikdar, F. Ore, J.H. Moore, Crystallization of calcium sulfate hemihydrate in reagent-grade phosphoric acid, AIChE Symp. Ser. 76 (193) (1978) 82–89.
[5] N. Touqan, Jordan Phosphate Mines Co., Research Center, Rusaifa, Jordan, 1995, private communication.
[6] A.V. Slack, Fertilizer Science and Technology Series, Vol. 1, Phosphoric Acid, Parts I and II, Marcel Dekker, New York, 1968.
[7] K. Shakourzadeh, R. Bloise, F. Baratin, Modeling of a wet-process phosphoric acid reactor: influence of phosphate rock impurities, in: Proceedings of the Second International Congress on Phosphorus Compounds, April 21–25, 1980, Boston, MA, pp. 443–455.
[8] F. Gioia, G. Mura, A. Viola, Analysis, simulation, and optimization of the hemihydrate process for the production of phosphoric acid from calcareous phosphorites, Ind. Eng. Chem. Process. Des. Dev. 16 (1977) 390–399.
[9] S. van der Sluis, Y. Meszaros, W.G.J. Marchee, H.A. Wesselingh, G.M. van Rosmalen, The digestion of phosphate ore in phosphoric acid, Ind. Eng. Chem. Res. 26 (1987) 2501–2505.
[10] R.L. Gilbert, E.C. Moreno, Dissolution of phosphate rock by mixtures of sulfuric and phosphoric acids, Ind. Eng. Chem. Process. Des. Dev. 4 (1965) 368–371.
[11] A.B. Amin, M.A. Larson, Crystallization of calcium sulfate from phosphoric acid, Ind. Eng. Chem. Process. Des. Dev. 7 (1968) 133–137.
[12] T.P. Hignett, Production of wet-process phosphoric acid, in: Proceedings of the Second International Congress on Phosphorus Compounds, April 21–25, 1980, Boston, MA, pp. 401–429.
[13] M. Al-Muthaker, N. Touqan, L. Dabbas, M. Tarawneh, Assessment of Eshidiya phosphate for phosphoric acid manufacture, in: Proceedings of the Jordanian Chemical Engineering Conference I, Vol. III, October 18–20, 1993, pp. 538–566.
[14] R.E. Treybal, Mass Transfer Operations, 3rd Edition, McGraw-Hill, Singapore, 1980.
[15] C.E. Calmanovici, N. Gabas, C. Laguerie, Solubility measurements for calcium sulfate dihydrate in acid solutions at 20, 50, and 70°C, J. Chem. Eng. Data 38 (1993) 534–536.